Multiscale Mechanics of Fibrin Polymer: Gel Stretching with Protein Unfolding and Loss of Water

André E. X. Brown, *et al.*

Science **325**, 741 (2009);
DOI: 10.1126/science.1172484

Multiscale Mechanics of Fibrin Polymer: Gel Stretching with Protein Unfolding and Loss of Water

André E. X. Brown,[1,2] Rustem I. Litvinov,[3] Dennis E. Discher,[2,4] Prashant K. Purohit,[5] John W. Weisel[3]*

Blood clots and thrombi consist primarily of a mesh of branched fibers made of the protein fibrin. We propose a molecular basis for the marked extensibility and negative compressibility of fibrin gels based on the structural and mechanical properties of clots at the network, fiber, and molecular levels. The force required to stretch a clot initially rises linearly and is accompanied by a dramatic decrease in clot volume and a peak in compressibility. These macroscopic transitions are accompanied by fiber alignment and bundling after forced protein unfolding. Constitutive models are developed to integrate observations at spatial scales that span six orders of magnitude and indicate that gel extensibility and expulsion of water are both manifestations of protein unfolding, which is not apparent in other matrix proteins such as collagen.

Fibrin clots are proteinaceous gels that polymerize in the blood as a consequence of biochemical cascades at sites of vascular injury. Together with platelets, this meshwork stops bleeding and supports active contraction during wound healing (*1*, *2*). Fibrin also provides a scaffold for thrombi, clots that block blood vessels and cause tissue damage, leading to myocardial infarction, ischemic stroke, and other cardiovascular diseases (*3*). To maintain hemostasis while minimizing the impact of thrombosis, fibrin must have suitable stiffness and plasticity (*4*), but also sufficient permeability so that the network can be effectively decomposed (lysed) by proteolytic enzymes (*5*, *6*). It is challenging to meet all of these conditions because open scaffolds would be expected to break at low strains, as is true for collagen gels (*7*). To address how fibrin clots are both permeable and highly extensible, we studied fibrin structures across multiple spatial scales, from whole clots to single fibers and single molecules (Fig. 1).

Fibrin clots were made from purified human fibrinogen under conditions (*8*) that resulted in the formation of long, straight fibers, similar to those found in physiological clots. To simplify the interpretation, the clots were covalently ligated with the use of a transglutaminase (blood clotting factor XIIIa), as naturally occurs in the blood, which prevents protofibrils from sliding past one another, thus eliminating persistent creep (*9*).

Measurements of the extensibility of 2-mm-diameter fibrin clots (Fig. 2A) demonstrated that the clots could be stretched to more than three times their relaxed length before breaking, with an average stretch of 2.7 ± 0.15–fold ($n = 6$) (*10*). This is comparable to the single-fiber extensibility that is observed when a fibrin fiber is laterally stretched with an atomic force microscope (*11*). Qualitatively, the resulting force-strain curve for fibrin is similar to those observed for rubbers and other materials made from flexible chains (*12*). However, for fibrin clots, which are made of longer, straighter fibers than the thermally fluctuating polymer chains in rubber, models of rubber-like elasticity predict a branching density that is wrong by seven orders of magnitude (*4*). Therefore, new models are needed to understand clot mechanics.

In addition to the large extensibility of fibrin clots, these gels also displayed a dramatic decrease in volume upon stretching [supporting online material (SOM) movie S1], unlike most rubbery materials. This unusual effect is quantified in Fig. 2B where the lateral contraction of the gel λ_* allows one to calculate the relative volume ($\lambda_1\lambda_*^2$), which is plotted as function of strain (black circles) and contrasted with a volume-conserving incompressible material (black dashed line). The shrinkage of the stretched clot was due to water expulsion, as confirmed by an ~10-fold increase in the protein content in clots at a strain of 2 (fig. S1B). This protein concentrating effect, or syneresis, is mechanically induced and corresponds to a negative compressibility for the gel (Fig. 2B, inset); the intrinsic compressibility of proteins is usually positive and small, ~2×10^{-4} MPa^{-1} (Fig. 2B inset, open circle) (*13*). This effect might be related to the phenomenon of negative normal stress observed for networks of semiflexible polymers, because even though fibrin fibers are relatively stiff, it is still possible that they buckle more easily than they stretch, thus leading to an effective inward force (*14*). However, our data below support an alternative explanation in which the volume change is associated with protein unfolding and bundling of stretched fibrin fibers.

To understand what makes fibrin so different from other highly extensible polymers, including rubbers and hydrogels, we quantified the structural changes that occur in stretched clots at the network and fiber levels. Unstrained clots imaged with the use of scanning electron microscopy have well-separated fibers with an essentially random orientation (Fig. 3A, top image). When strain is applied (Fig. 3A, lower images), the fibers begin to align and the network orientational order parameter (*15*) increases gradually from 0.1 to 0.7 at a strain of ~2.5 (Fig. 3B).

Transmission electron microscopy of transverse sections through fibrin clots at increasing strain (Fig. 3C, insets) provides a clear picture

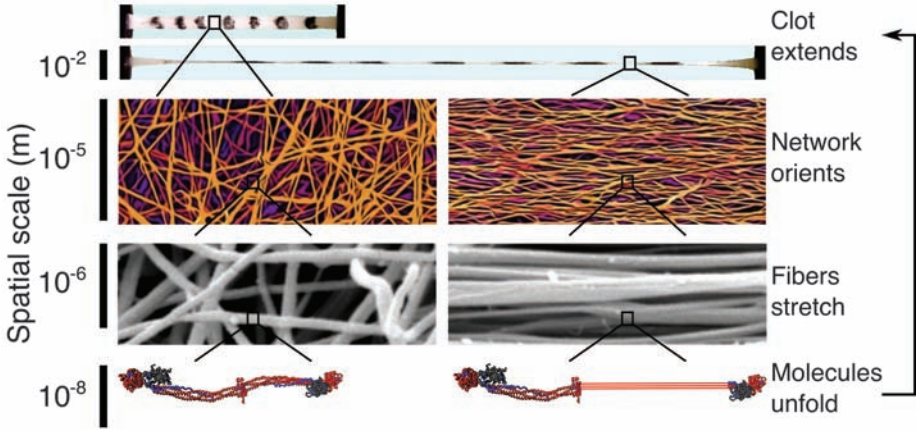

Fig. 1. Blood clots are highly extensible supramolecular protein polymers formed from well-separated, relatively straight and stiff fibers ~200 nm in diameter. When stretched (see movie S1), the fiber network aligns in the direction of the applied strain and the individual fibers stretch, forcing the fibrin monomers that make up the fibers to extend. Ultimately, it is this molecular unfolding that allows clots to stretch so far. Thus, understanding fibrin clot mechanics requires knowledge of the mechanical response and the corresponding structural changes spanning from the centimeter scale to the nanometer scale.

[1]Department of Physics and Astronomy, University of Pennsylvania, Philadelphia, PA 19104, USA. [2]Nano/Bio Interface Center, University of Pennsylvania, Philadelphia, PA 19104, USA. [3]Department of Cell and Developmental Biology, University of Pennsylvania School of Medicine, Philadelphia, PA 19104, USA. [4]Graduate Groups in Physics and Cell Biology and Physiology, University of Pennsylvania, Philadelphia, PA 19104, USA. [5]Department of Mechanical Engineering and Applied Mechanics, University of Pennsylvania, Philadelphia, PA 19104, USA.

*To whom correspondence should be addressed. E-mail: weisel@mail.med.upenn.edu

of how the fibers become thinner, closer together, and bundle. The area occupied by fibers increases from ~5 to 24% at a strain of 2 (Fig. 3C, graph). This increase is smaller than expected given the macroscopic shrinkage of the entire clot (see SOM), indicating that the volume decrease is a combined result of fiber bundling and a decrease in fiber diameter from 185 ± 36 to 74 ± 16 nm (mean ± SD, $P << 0.0001$, Student's t test). Similar transmission electron micrographs (although without corresponding scanning electron micrographs) of fiber ordering have been reported (*16*), but quantifying the strain dependence of these observations proves important below in constraining possible models. Furthermore, knowing the stress applied and the fractional cross section occupied by fibers allows for an estimate of the force per protofibril of ~75 pN at a strain of 2. Given the small loading rate that we used, this force is large enough to result in substantial unfolding of fibrin (*17*). Protein unfolding is generally associated with increased exposure of hydrophobic groups that would tend to interact (e.g., bundle) and expel water, as observed here.

The half-staggered packing of fibrin (Fig. 4A) leads to a ~22-nm repeat that can be measured by small-angle x-ray scattering (SAXS), and this measurement can be used as a readout of the molecular length (*18*). The position of the peak corresponding to the 22-nm spacing does not change substantially as the clot is stretched (Fig. 4B), ruling out a gradual extension of molecules during the stretch, which would otherwise increase this spacing, as suggested by Roska *et al*. (*19*). The marked increase in peak width that we observed indicates an increase in disorder that is consistent with an increasing number of molecules unfolding in response to the large strain. This increase in disorder is captured by the decrease in the Scherrer length L (Fig. 4C): The length over which the 22-nm repeat is correlated (*20*). A decrease in L indicates that the average size of the regions containing a consistent 22-nm repeat becomes smaller because of intervening regions of unfolded molecules. To control for the effect on L of fiber alignment that accompanies strain, we made magnetically prealigned samples in which the fibers were already oriented along the direction of applied strain. In this case, the decrease in L occurs at lower strains because fiber alignment cannot take up as much of the applied strain (Fig. 4C, blue circles). This change is reversible when fibers are allowed to relax (Fig. 4C, blue arrow). Similarly, to control for fiber sliding as an alternative mechanism of strain accommodation, we stretched samples that were not covalently ligated using factor XIIIa. Without ligation, protofibrils slide with respect to each other instead of stretching, and unfolding is suppressed (Fig. 4C, black circles). This behavior is expected for two-state extension in which some molecules extend completely while others remain folded, consistent with our earlier single-molecule observations of the forced unfolding of coiled coils

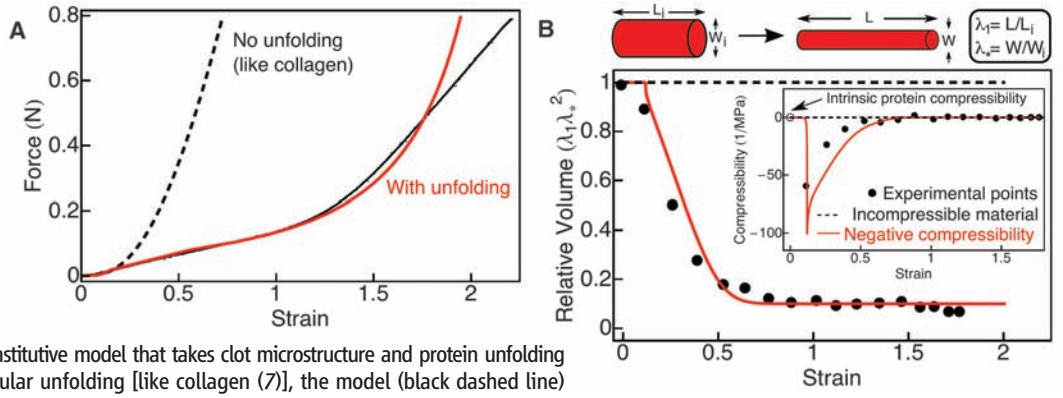

Fig. 2. (**A**) Representative force-extension curve of a cylindrical fibrin clot reaching a threefold longitudinal stretch. The average stretch before breaking was 2.7 ± 0.15–fold (mean ± SEM, $n = 6$ experiments). As the strain (stretched length/initial length − 1) increases, the force on the clot increases linearly until a strain of ~1.2 is reached, at which point the sample hardens and enters a new regime with a steeper slope (black solid line). The force-extension curve (black solid line) is fit using a constitutive model that takes clot microstructure and protein unfolding into account (red line). Without molecular unfolding [like collagen (*7*)], the model (black dashed line) rapidly diverges from the experimental data (black solid line). (**B**) The relative clot volume decreases with strain (black circles), in contrast to the behavior of an incompressible material (dashed black line). This decrease is predicted with the use of the same model and parameters that we used to fit the force-extension data (red line), demonstrating that the volume decrease occurs in parallel with molecular extension (SOM Eq. 29). A decreasing volume with increasing stretch corresponds to a negative compressibility (inset), which indicates that there is a source of free energy to drive contraction, possibly due to fiber bundling when hydrophobic side chains aggregate and bury after exposure during unfolding. The negative compressibility is a property of the network. Proteins in solution have been observed to have intrinsic compressibilities ~2×10^{-4} MPa^{-1} (open circle, inset) (*13*). L, length; L_i, initial length; W, width; W_i, initial width.

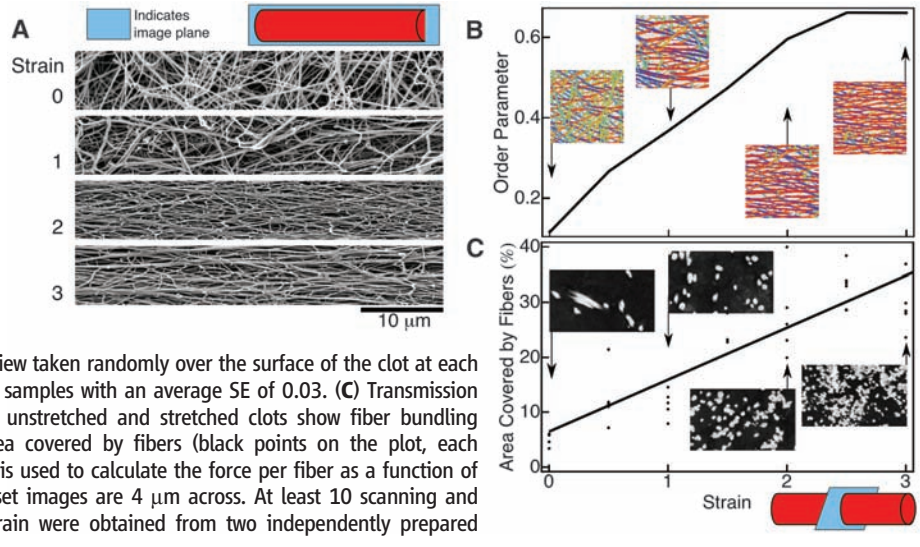

Fig. 3. Structural changes in stretched fibrin clots at the network and fiber levels. Scanning electron micrographs of stretched clots (**A**) show how the fibrin fibers align with strain. (**B**) These scanning electron micrographs are segmented using a Laplace of Gaussian filter that determines which pixels are fibers and which are background and also calculates the orientation θ at each fiber pixel. The inset images show the results of the segmentation with the color at each pixel corresponding to that pixel's orientation. These data are summarized as an orientational order parameter <cos(2θ)> that can range between 0 for randomly oriented fibers and 1 for perfectly aligned fibers (*14*). Data points are averages of five fields of view taken randomly over the surface of the clot at each strain. The order parameter was fairly uniform across samples with an average SE of 0.03. (**C**) Transmission electron micrographs of transverse sections through unstretched and stretched clots show fiber bundling (insets). The plot shows the total cross-sectional area covered by fibers (black points on the plot, each representing a randomly chosen field of view), which is used to calculate the force per fiber as a function of strain from the total force applied to the sample. Inset images are 4 μm across. At least 10 scanning and transmission electron microscope images at each strain were obtained from two independently prepared samples with similar results.

in fibrinogen oligomers (*17*). A more gradual unfolding has been observed in molecular dynamics simulations (*21*), but the coiled-coil spanning αC region is missing from published crystal structures of fibrinogen and is therefore not included in the simulation. Early wide-angle x-ray scattering measurements of fibrin clots support this view of molecular extension (*22*), providing evidence for a folding transition from α helix to β sheet, as has been observed for stretched keratin (*23*, *24*).

When these results are taken together, the following picture of fibrin mechanics emerges (Fig. 1). Because fibrin fibers are straight and relatively stiff, thermally induced bends are negligible, and so there is no slack to be pulled out upon extension. Instead, even at relatively low strains, the fibers themselves must begin to orient and stretch along the direction of the applied strain. The volume fraction of protein within the fibers has been estimated at ~20% (*25*), and the protofibrils that make up the fibers are known to adopt a twisted conformation (*26*) so that, at low strains, fibers could stretch somewhat by having protofibrils straighten and untwist within the fibers. However, to reach even a strain of ~0.15, unfolding must start to play a role. It is this structural transition that allows fibrin clots to maintain their linear response until strains of 1.2, at which point the coiled coils, or perhaps some other compact structures, are stretched to near their unfolded contour lengths, leading to strain hardening. The unfolded domains then interact and expel water, as many denatured proteins do.

To quantitatively test this mechanism, two approaches to model the stress-strain behavior of networks of semi-flexible filaments can be adapted for fibrin. A first model for random networks of folded proteins (*27*) uses a system of connected fibers. Although this model is not explicitly based on the microscopic structure of the network, it has been shown to accurately describe other random networks and serves to connect the microscopic and macroscopic processes. This leads to an expression for the force-extension (or stress-strain) relation of the network in terms of the force-extension relation of a single fiber. The molecules making up the fiber are modeled as two-state systems that can be either folded, in which case the fiber behaves as a linear spring, or unfolded, in which case it is modeled as a wormlike chain (*28*) (see SOM).

An alternative model of filamentous gels starts from the assumption that the networks are homogeneous and isotropic, and strain uniformly (*29*). Such a model can be used to compute the mechanical properties of the network after choosing a fiber force-extension curve as above. This model captures the trend in the data if buckling is taken into account by setting the force on a fiber to zero whenever it is under compression.

With either modeling approach, protein unfolding is required to fit the experimental data. Without unfolding, the fit rapidly diverges from the experimental force-extension curve (Fig. 2A, black dashed line). The fraction of folded domains n_f determined from the model correlates with the decreasing Scherrer length L observed with SAXS (Fig. 4D), providing further evidence that sample disordering is due to molecular extension. The divergence at high strains is probably due to unfolding of structures in the fibrin molecules other than coiled coils, which has been suggested as a possible mechanism to account for the extensibility of single fibrin fibers (*11*) and could be straightforwardly incorporated into our model to fit the force-extension data at the highest strains. In contrast, a linear model without unfolding fits collagen force extension data reasonably well (see SOM). This further highlights the uniqueness of fibrin's ability to balance large extensibility with a large pore size.

To account for the measured volume change in addition to the other results, we modified the first model (*27*) by associating a volume decrease with the unfolding transition. By matching the volume change at high strain, we determined the fractional volume change per domain and then, with no further fitting, the observed volume drop at low strain was captured using the same parameters as those used to fit the force-extension curve (compare Figs. 2B and 4D). The approximate fit to the negative peak in the compressibility (Fig. 2B, inset) further increases confidence in the model and again suggests a connection between clot shrinkage and an unfolding transition (SOM Eq. 29). A likely mechanism is aggregation that buries hydrophobic residues exposed during forced unfolding of protein (fig. S3).

Thus, it is the molecular extensibility of fibrin that allows clots' long straight fibers to extend and that endows them with essential properties, such as large pore sizes and low fibrin volume fraction in combination with extensibility. This allows for efficient permeation and lysis of clots (*5*) and maintenance of mechanical integrity in dynamic environments (e.g., platelet-induced clot retraction, skin and internal wounds that could stretch during healing, arterial thrombi, and pulsatory thrombotic aneurysms). The fact that these molecular transitions occur at small strains that cells can exert (*30*) and are manifested directly in the macroscopic mechanics of fibrin may represent a clear example of an important biological function of forced protein unfolding, as also

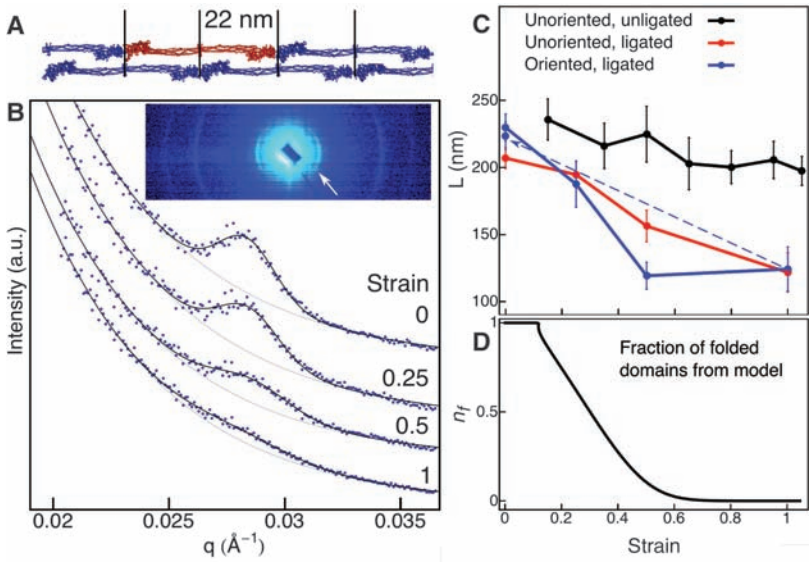

Fig. 4. Structural changes in stretched fibrin clots at the molecular level. (**A**) Schematic of a fibrin protofibril showing the half-staggered pattern that leads to a characteristic 22-nm repeat. A fibrin monomer within the protofibril is shown in red. (**B**) SAXS from fibrin clots leads to a clear first-order peak (white arrow, inset) and to third- and fourth-order peaks. The plots show the peak shape as a function of the wave vector $q = 2\pi/d$, which increases radially from the center (here, d is the fibrin periodicity, 22 nm). The thick lines are fits to the data using the sum of an exponential and a Gaussian with the exponential alone (thin lines) shown for comparison. The width of the peak increases with increasing stretch, which can be understood in terms of a two-state–like extension of fibrin molecules that introduce defects into the sample. a.u., arbitrary units. (**C**) This effect is quantified as the Scherrer length L, which decreases with increasing strain (red). The decrease is more rapid for samples that were prealigned in a magnetic field during polymerization (blue), which implies that network alignment accommodates some strain and delays unfolding. The transition is reversible when samples are allowed to relax, as indicated by the blue arrow. When samples are not ligated using factor XIIIa, protofibril sliding becomes important, and unfolding is decreased. In all cases, the peak position remains relatively constant, implying that there is no gradual lengthening of the whole population of fibrin monomers. Instead, there remains a population that is not unfolded and maintains a fairly constant spacing. Error bars indicate SDs of the distribution of L determined from fits using the bootstrap method. This bootstrap error is similar to the average SE of 15 nm calculated by averaging over results from four samples. (**D**) This behavior is captured by the constitutive model in which the fraction of folded monomers n_f decreases with increasing strain.

demonstrated for some proteins in stressed cells (*31*). Unfolded domains could be promising targets for modification in applications such as tissue engineering and cell biophysics, where stiffness is known to be important (*30*), and for designs of tougher fibrin sealants used in surgeries (*32*). Controlling unfolding could also lead to new strategies for breaking thrombi, perhaps by stabilizing the coiled coil, rendering clots more brittle for thrombectomy, or by destabilizing the coiled coil, making clots softer and less occlusive. Structural transitions observable at multiple scales may also be involved in the mechanics of other protein assemblies.

References and Notes

1. J. W. Weisel, in *Advances in Protein Chemistry*, vol. 70 (Academic Press, London, 2005), pp. 247–299.
2. N. Laurens, P. Koolwijk, M. P. M. DeMaat, *J. Thromb. Haemost.* **4**, 932 (2006).
3. R. W. Colman *et al.*, *Hemostasis and Thrombosis: Basic Principles and Clinical Practice* (Lippincott Williams & Wilkins, Philadelphia, 2005).
4. J. W. Weisel, *Biophys. Chem.* **112**, 267 (2004).
5. J. P. Collet *et al.*, *Arterioscler. Thromb. Vasc. Biol.* **20**, 1354 (2000).
6. D. A. Gabriel, K. Muga, E. M. Boothroyd, *J. Biol. Chem.* **267**, 24259 (1992).
7. B. A. Roeder *et al.*, *J. Biomech. Eng.* **124**, 214 (2002).
8. Materials and methods are available as supporting material on *Science* Online.
9. P. A. Janmey, E. J. Amis, J. D. Ferry, *J. Rheol.* **27**, 135 (1983).
10. The clots typically break where they are clamped, suggesting that the true clot extensibility is larger than that measured here.
11. W. Liu *et al.*, *Science* **313**, 634 (2006).
12. L. R. G. Treloar, *The Physics of Rubber Elasticity* (Clarendon, Oxford, 1975).
13. D. P. Kharakoz, *Biophys. J.* **79**, 511 (2000).
14. H. Kang *et al.*, *J. Phys. Chem. B* **113**, 3799 (2009).
15. The orientational order parameter is defined as $\langle \cos 2\theta \rangle$, where θ is the angle of the fiber determined at each fiber pixel (see SOM for a description of the analysis algorithm).
16. M. F. Müller, H. Ris, J. D. Ferry, *J. Mol. Biol.* **174**, 369 (1984).
17. A. E. X. Brown, R. I. Litvinov, D. E. Discher, J. W. Weisel, *Biophys. J.* **92**, L39 (2007).
18. L. Stryer, C. Cohen, R. Langridge, *Nature* **197**, 793 (1963).
19. F. J. Roska, J. D. Ferry, J. S. Lin, J. W. Anderegg, *Biopolymers* **21**, 1833 (1982).
20. L. E. Alexander, *X-Ray Diffraction Methods in Polymer Science* (Wiley, Hoboken, NJ, 1979).
21. B. B. C. Lim, E. H. Lee, M. Sotomayor, K. Schulten, *Structure* **16**, 449 (2008).
22. K. Bailey, W. T. Astbury, K. M. Rudall, *Nature* **151**, 716 (1943).
23. W. T. Astbury, H. J. Woods, *Proc. R. Soc. London Ser. B Biol. Sci.* **114**, 314 (1934).
24. J. W. S. Hearle, *Int. J. Biol. Macromol.* **27**, 123 (2000).
25. W. A. Voter, C. Lucaveche, H. P. Erickson, *Biopolymers* **25**, 2375 (1986).
26. J. W. Weisel, C. Nagaswami, L. Makowski, *Proc. Natl. Acad. Sci. U.S.A.* **84**, 8991 (1987).
27. H. J. Qi, C. Ortiz, M. C. Boyce, *J. Eng. Mater. Technol.* **128**, 509 (2006).
28. C. Bustamante, J. F. Marko, E. D. Siggia, S. Smith, *Science* **265**, 1599 (1994).
29. C. Storm *et al.*, *Nature* **435**, 191 (2005).
30. D. E. Discher, P. Janmey, Y.-l. Wang, *Science* **310**, 1139 (2005).
31. C. P. Johnson, H.-Y. Tang, C. Carag, D. W. Speicher, D. E. Discher, *Science* **317**, 663 (2007).
32. D. M. Albala, *Cardiovasc. Surg.* **11**, 5 (2003).

33. We thank P. Heiney for help with the x-ray diffraction measurements (NSF–Materials Research Science and Engineering Center partial support); C. Nagaswami for scanning electron microscopy; D. Galanakis for his gift of fibrinogen; S. Pickup for access to the magnet facility; A. Kota for help with the tensile testing; J. Torbet for discussions of x-ray diffraction and magnetic alignment; and P. Janmey, T. Lubensky, H. Shuman, and C. Storm for useful discussions. This work was supported by NIH (grants HL090774 and HL30954 to J.W.W. and grant HL62352 to D.E.D.) and by the Nano/Bio Interface Center through NSF Nanoscale Science and Engineering Center (grant DMR-0425780). A.E.X.B. was supported by a scholarship from the Natural Sciences and Engineering Research Council of Canada.

Supporting Online Material

www.sciencemag.org/cgi/content/full/325/5941/741/DC1
Materials and Methods
SOM Text
Figs. S1 to S11
References
Movie S1

18 February 2009; accepted 19 June 2009
10.1126/science.1172484

The C-Ala Domain Brings Together Editing and Aminoacylation Functions on One tRNA

Min Guo, Yeeting E. Chong, Kirk Beebe,* Ryan Shapiro, Xiang-Lei Yang, Paul Schimmel†

Protein synthesis involves the accurate attachment of amino acids to their matching transfer RNA (tRNA) molecules. Mistranslating the amino acids serine or glycine for alanine is prevented by the function of independent but collaborative aminoacylation and editing domains of alanyl-tRNA synthetases (AlaRSs). We show that the C-Ala domain plays a key role in AlaRS function. The C-Ala domain is universally tethered to the editing domain both in AlaRS and in many homologous free-standing editing proteins. Crystal structure and functional analyses showed that C-Ala forms an ancient single-stranded nucleic acid binding motif that promotes cooperative binding of both aminoacylation and editing domains to $tRNA^{Ala}$. In addition, C-Ala may have played an essential role in the evolution of AlaRSs by coupling aminoacylation to editing to prevent mistranslation.

The algorithm of the genetic code is established in the first reaction of protein synthesis. In this reaction, aminoacyl–transfer RNA (tRNA) synthetases (AARSs) catalyze the attachment of amino acids to their cognate tRNAs that bear the triplet anticodons of the genetic code. When a tRNA is acylated with the wrong amino acid, mistranslation occurs if the misacylated tRNA is released from the synthetase, captured by elongation factor, and used at the ribosome for peptide synthesis. To prevent mistranslation, some AARSs have separate editing activities that hydrolyze the misacylated amino acid from the tRNA (*1*–*3*). Because an editing-defective tRNA synthetase is toxic to bacterial and mammalian cells (*4*, *5*) and is causally linked to disease in animals (*6*), strong selective pressure retains these editing activities throughout evolution.

A particular challenge appears to be avoiding mistranslation of serine or glycine for alanine. All three kingdoms of life contain free-standing editing-proficient homologs of the editing domains found in alanyl-tRNA synthetases (AlaRSs) (*7*). These proteins, known as AlaXps, provide functional redundancy by capturing mischarged $tRNA^{Ala}$ molecules that escape the embedded editing activities of AlaRSs (*8*). Although free-standing editing domains have counterparts in ThrRS and ProRS (*7*, *9*, *10*), they are not as evolutionarily conserved as AlaXps. Moreover, enzymes like LeuRS, IleRS, and ValRS lack any free-standing editing domain counterparts (*1*, *2*, *11*, *12*). Despite the multiple checkpoints to prevent mischarging of $tRNA^{Ala}$, we did not know how the apparatus for preventing confusion of serine and glycine for alanine was assembled. To pursue this question, we focused on a third domain separate from the editing and aminoacylation domains, known as C-Ala, which is found in all AlaRSs and is tethered to their editing domains.

The modular arrangement of domains in AlaRSs is evolutionarily conserved (*13*) (Fig. 1A). The N-terminal aminoacylation domain is active as an isolated fragment, and its three-dimensional structure is that of a typical class II AARS. The central editing domain is homologous to the editing domain of the class II ThrRS (*14*, *15*). Lastly, a linker tethers the third (C-Ala) domain to the editing domain. In contrast to the other two domains, C-Ala is only loosely conserved and its structure is unknown. On the basis of a survey of AlaRS sequences, we predicted that a fragment corresponding to residues 766 to 875 of *Escherichia coli* AlaRS would form a structural unit (Fig. 1B). The corresponding region of *Aquifex aeolicus* AlaRS is the 110–amino acid fragment encompassing residues 758 to 867, which was expressed in *E. coli*, purified, and crystallized (*16*). The structure was solved to a resolution of 1.85 Å

The Skaggs Institute for Chemical Biology and the Department of Molecular Biology, The Scripps Research Institute, BCC-379, 10550 North Torrey Pines Road, La Jolla, CA 92037, USA.

*Present address: Metabolon, Incorporated, 800 Capitola Drive, Suite 1, Durham, NC 27713, USA.

†To whom correspondence should be addressed. E-mail: schimmel@scripps.edu